3D visualisation of AVO anomalies

Anat Canning, Alex Litvin and Lucy Eastwood of geoscience software and services company Paradigm Geophysical make the case for multi-attribute visualization techniques in the analysis of large AVO data sets claiming faster detection of hydrocarbon anomalies.

Introduction

AVO inversion of 3D data leads to generation of multiple volume attributes. In the case of Shuey–Hilterman formulation Intercept and Gradient volumes are generated. In the case of Aki–Richards formulation the inversion process generates P and S wave reflectivity volumes. In addition to these primary attributes a number of secondary attributes are generated (For example: Constrained gradient, pseudo-Poisson reflectivity, Fluid factor etc.). For confident identification of AVO anomalies the interpreter has to work simultaneously with these multiple 3D attribute volumes. This is an inherent difference between the interpretation of conventional seismic cubes and the interpretation of 3D AVO data.

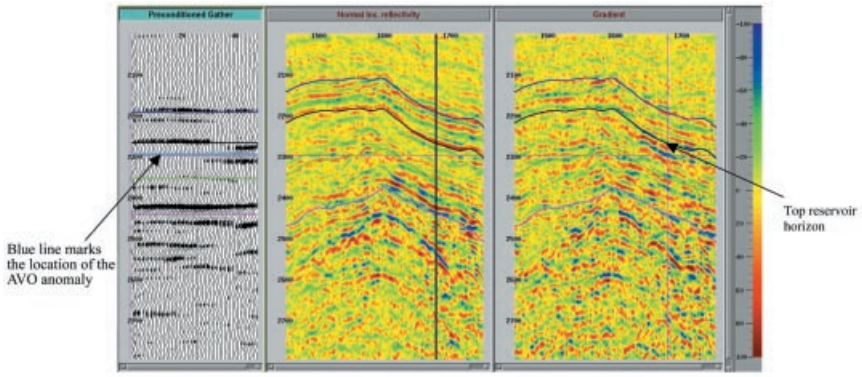

Figure 1

In this paper we will present two approaches to combined visualisation of 3D AVO attributes generated by the application of Shuey–Hilterman inversion scheme to the 3D pre-stack time migrated data set from the North Sea. The first approach uses multi-attribute volume visualisation of AVO attributes. The second approach uses cross-plot based volume visualisation.

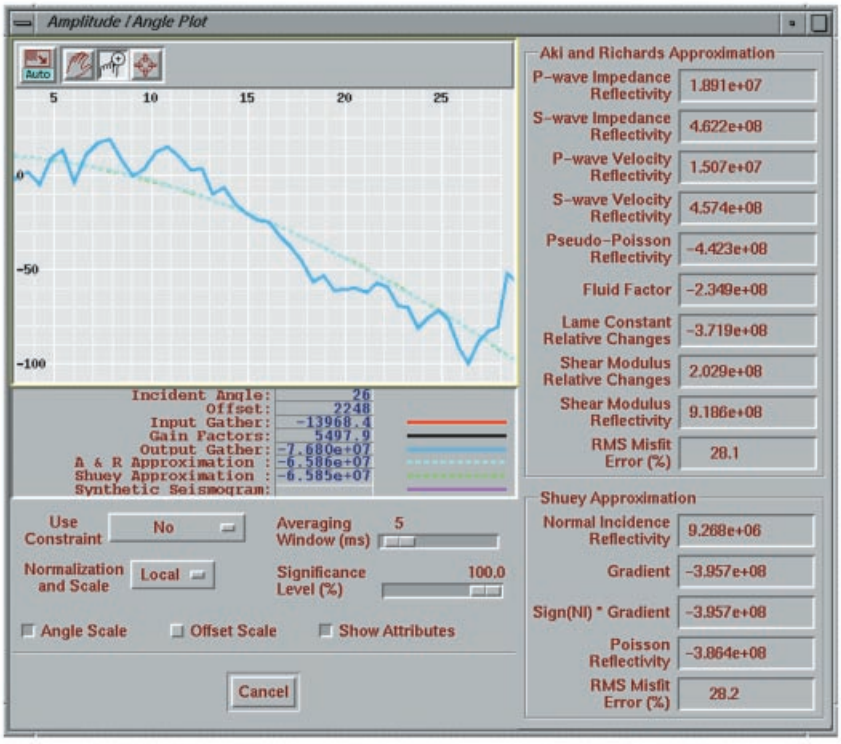

Figure 2

Multi-attribute volume visualisation approach

In this approach we use voxel-based visualisation where a separate colour table and opacity are defined for each type of AVO attribute. Figure 1 is a combined display with the left panel showing an example gather, the central panel showing the normal incidence reflectivity (NI) and the rightmost panel showing the gradient (G) attribute.

The vertical line on the NI section marks the location of the gather. The black picked horizon (showing on both sections) indicates smoothed top reservoir. Well-based synthetic modelling shows that the presence of hydrocarbons generates a Class II AVO anomaly (polarity changing from near to far offsets) with a large AVO gradient. This anomaly is clearly seen on the gather. Fig. 2 presents the amplitude versus an-

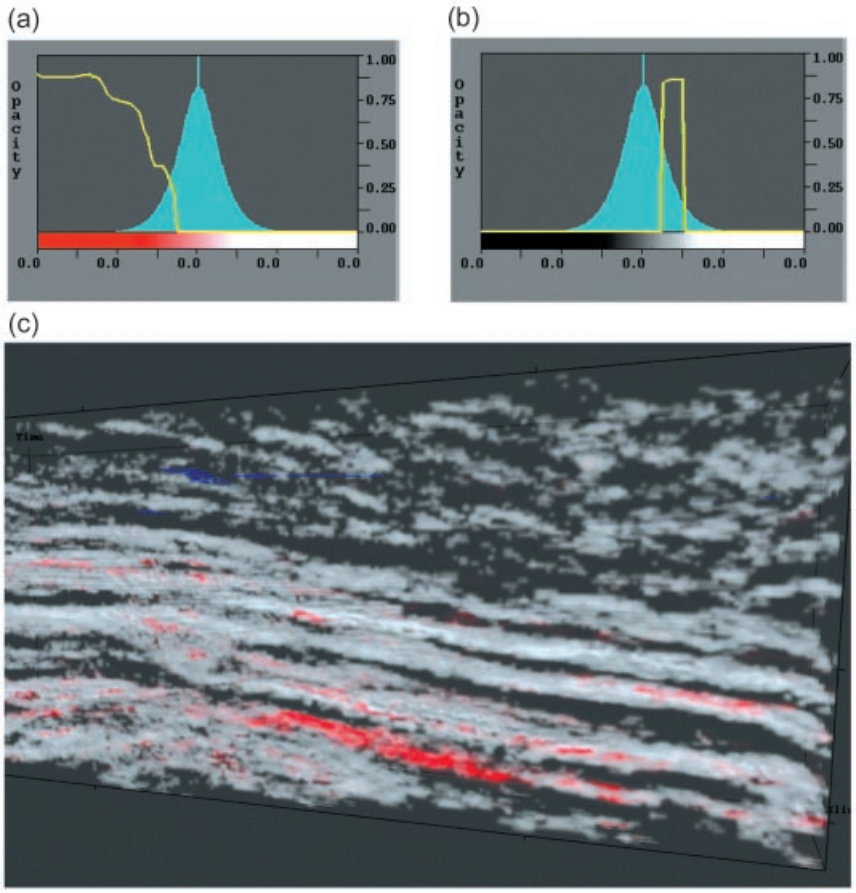

Figure 3

gle curve for the event indicated by the light blue line on the gather.

The blue curve shows the seismic amplitude extracted from the gather, the dashed magenta line shows the best-fitt approximation. In this particular case Aki–Richards and Shuey–Hilterman formulations give very close approximation for the survey angle range. We see that the AVO anomaly is characterised by a relatively small positive normal incidence reflectivity with a large negative gradient. Shuey attribute values are shown on the right bottom part of Figure 2. This type of AVO cor-

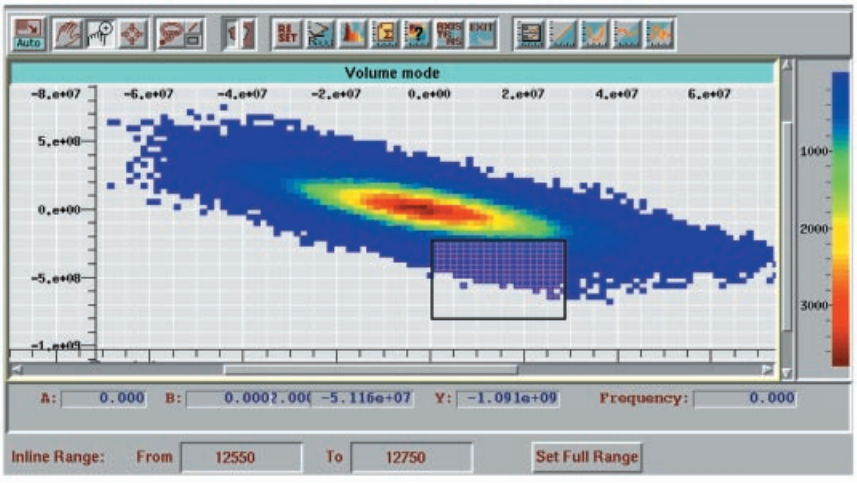

Figure 4

responds to low-intermediate positive NI values and large negative G values. For the interpretation of this dataset, both NI and G volumes are rendered together. We set the opacity control as shown in Figs 3a (for G volume) and 3b (for NI volume). The black-white colour table is used for the NI volume and the red-white table for the G volume. The display of the G volume is superimposed on the NI volume and is shown in Fig. 3c.

Red (negative) gradient anomaly coinciding with intermediate positive (light-grey) NI values can be clearly seen. This display allows the interpreter to benefit from both the continuity of events that exists on the NI dataset and the amplitude variations on the G data set, which mark the potential location of hydrocarbons. This type of analysis allows the separation of stratigraphic and hydrocarbon-related AVO anomalies. For stratigraphic anomalies high G values will correspond to high NI values that can lead to different overlapping on the display.

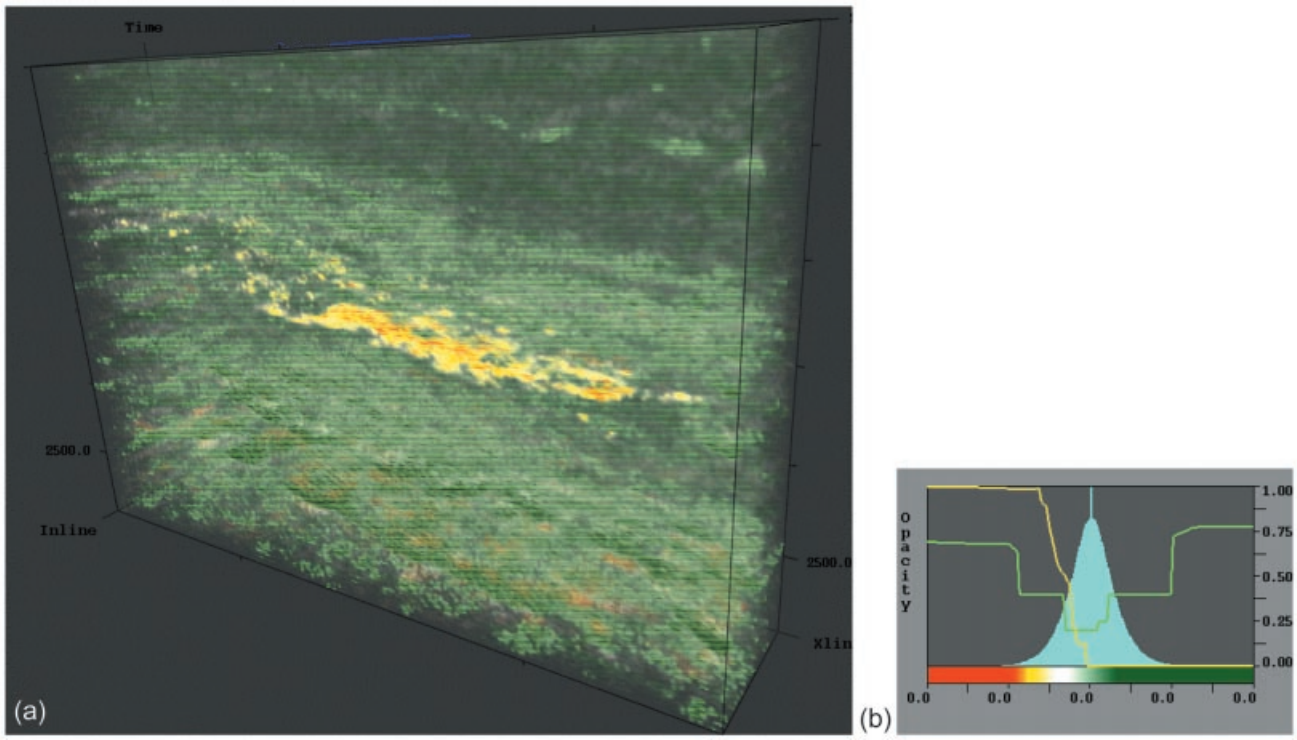

Figure 5

Cross-plot-based visualisation approach

With AVO anomalies the interpreter is looking for a specific relationship between two attributes more than he is interested in analysing specific events on the individual attribute sections. To aid with this process we use sub-volume detection driven by a cross-plot of 3D AVO attributes. In Fig. 4 we cross-plotted G (vertical axes) and NI (horizontal axes) attribute volumes. The data range for cross-ploting was limited to a time interval of approximately 150 ms centred around the top reservoir.

The selected rectangle indicates an area where the relationship between the two attributes corresponds to a hydrocarbon related AVO effect (low-intermediate positive NI values and large negative G values). Voxels from the two volumes that satisfy the defined condition are marked as detected. A separate colour and opacity control can be applied to the detected voxels in order to make them more visible. The detected spatial anomaly is superimposed on the gradient volume and is shown in Fig. 5a in a light yellow colour. We used the same colour table for both the detected anomaly and the gradient volume, but applied different opacity controls for the detected (yellow curve) and the undetected (green curve) data (Fig. 5b). Variable opacity of detected voxels allows better visualisation of the internal structure of the AVO anomaly and shows lateral gradient variations within the detected subvolume.

Conclusion

These multi-attribute visualisation techniques make the analysis of large AVO data sets more accurate and far more effective than conventional single volume line-by-line analysis. Multi-attribute visualisation allows fast detection of the hydrocarbon-related anomalies. More detailed analysis of CRP gathers can be performed for further validation of the detected anomaly.